Effect of xeroderma pigmentosum group C on the characteristics and regulatory mechanisms of lung cancer stem cells

BEN YANG[1*], YANG YANG[2*], WEIYU WANG[3], YUBING WANG[1,4], HUAIJIE WANG[1], LIYA QIN[1], YONGMING WANG[1,5], SIPENG SUN[1], SHUBO WANG[5] and MEIHUA QU[1,4]

[1]Translational Medical Center, Weifang Second People's Hospital, Weifang Respiratory Disease Hospital, Weifang, Shandong 261041, P.R. China; [2]School of Public Health, Shandong Second Medical University, Weifang, Shandong 261053, P.R. China; [3]Department of Otolaryngology and Head and Neck Surgery, Shandong Provincial ENT Hospital, Jinan, Shandong 250022, P.R. China; [4]School of Life Science and Technology, Shandong Second Medical University, Weifang, Shandong 261053, P.R. China; [5]Department of Thoracic Surgery, Weifang Second People's Hospital, Weifang Respiratory Disease Hospital, Weifang, Shandong 261041, P.R. China

Received January 29, 2026; Accepted July 21, 2026

DOI: 10.3892/ijo.2026.5933

Abstract. Lung cancer is one of the most common and deadly forms of cancer worldwide, with >80% of cases being non-small cell lung cancer. Its recurrence and drug resistance have been major challenges in clinical treatment, posing a serious threat to the lives of patients. The present study found that high xeroderma pigmentosum group C (XPC) expression markedly reduced the proliferation capacity and stem cell characteristics of the lung cancer cell lines A549-XPC and H460-XPC. In addition, XPC overexpression led to a decreased in the proportion of cells in the G_2/M phase proportion, suggesting alterations in the cell cycle process. MTS assays showed that XPC overexpressing cells demonstrated markedly higher sensitivity to chemotherapy drugs compared with control cells. Furthermore, the clonogenic and anchorage-independent spheroid formation capacities of the cells were markedly inhibited with high XPC expression and the phosphorylation levels of the JAK/STAT pathway and the expression levels of stemness-associated markers were markedly altered. *In vivo* studies validated the effect of high XPC expression on tumorigenicity using a subcutaneous tumor model, with tumor volumes of 134.04±46.77 mm^3 and 324.64±85.31 mm^3 and weights of 164.24±76.16 mg and 434.70±115.72 mg for subcutaneously injected A549-XPC and A549-CTR cells, respectively. High expression of XPC in the A549 cells significantly affected tumor volume ($P<0.05$) and weight ($P<0.01$) *in vivo*. The present findings suggested that high XPC expression is associated with reduced proliferation, migration and stem cell-like properties in lung cancer cells, enhances their sensitivity to chemotherapy drugs and suppresses tumor growth *in vivo*. These observations supported further investigation of XPC as a potential therapeutic target and prognostic marker for lung cancer, offering new strategies to improve treatment outcomes and prolong patient survival.

Correspondence to: Professor Meihua Qu, Translational Medical Center, Weifang Second People's Hospital, Weifang Respiratory Disease Hospital, 7 Yuanxiao Street, Weifang, Shandong 261041, P.R. China
E-mail: qumeihua2016@163.com

Professor Shubo Wang, Department of Thoracic Surgery, Weifang Second People's Hospital, Weifang Respiratory Disease Hospital, 7 Yuanxiao Street, Weifang, Shandong 261041, P.R. China
E-mail: lanjian1993@163.com

*Contributed equally

Key words: xeroderma pigmentosum group C, lung cancer stem cell, JAK/STAT signaling pathway, chemotherapy

Introduction

Lung cancer is the leading malignant tumor in terms of incidence and mortality globally, and is primarily treated with surgery, chemotherapy, targeted therapy and immunotherapy (1). However, these treatments face challenges such as tumor recurrence, metastasis and drug resistance (2,3). A growing body of evidence suggests that lung cancer stem cells (LCSCs) are a rare subpopulation with the ability to self-renew and differentiate in multiple directions and may be a key factor contributing to tumor heterogeneity, metastasis and drug resistance (4). A study has demonstrated that LCSCs drive tumor growth, proliferation, metastasis, and recurrence (5). The self-renewal ability of LCSCs maintains the lung cancer cell population, even during treatment, while their multilineage differentiation potential causes tumor heterogeneity, complicating treatment efficacy (6).

Xeroderma pigmentosum group C (XPC) binds to damaged DNA to initiate repair and is vital in nucleotide excision repair (NER) (7,8). XPC has binding sites for OCT-4 and SOX2 (9,10). As the most genomically diverse malignant tumor, lung cancer relies on DNA repair pathways, especially NER, which are required for maintaining tumor diversity (11,12). XPC dysfunction or abnormal expression increases

DNA damage accumulation, leading to genomic instability and tumor development (13). In numerous tumor types, low XPC gene expression is linked to poor prognosis, highlighting its role in preserving genomic stability and suppressing tumor growth (14-16).

The JAK/STAT signaling pathway, particularly the JAK2/STAT3 pathway, has been widely recognized as a key regulator of stemness in various malignant tumors (17-19). Sustained activation of STAT3 maintains the self-renewal capacity of cancer stem cells and promotes their resistance to conventional chemotherapy (20,21). Notably, SOX2, a key stemness marker directly regulated by STAT3, has been shown to be involved in the maintenance of LCSCs (22-24). Given the interaction between XPC and SOX2, and the fact that STAT3 regulates SOX2 expression through transcription, it was hypothesized that XPC may modulate LCSC characteristics via the JAK2/STAT3/SOX2 axis (25).

Although previous studies have confirmed that XPC is a tumor suppressor gene in lung adenocarcinoma and demonstrated its influence on chemotherapy sensitivity, the specific role of XPC in the biology of LCSCs and its underlying molecular mechanisms remain unclear (26-30). In particular, three questions remain unresolved: Whether XPC overexpression inhibits LCSC self-renewal and tumorigenicity; whether XPC specifically regulates the chemotherapeutic sensitivity of the LCSCs population; and which signaling pathways mediates XPC-dependent LCSCs regulation. Our previous study (15) has shown that downregulating XPC in tumor cells via short hairpin (sh)RNA enhances tumor stemness and upregulates related molecular markers. A549 (lung adenocarcinoma) and H460 (large cell lung carcinoma) are well-established non-small cell lung cancer (NSCLC) cell lines with moderate endogenous XPC expression, making them suitable for investigating the effects of XPC overexpression on stem cell characteristics and chemotherapy sensitivity. Therefore, the present study established XPC-overexpressing cell lines for *in vitro* functional and *in vivo* xenograft model studies and it was demonstrated that elevated XPC expression attenuates the characteristics of LCSCs manifested as reduced spheroid formation, decreased expression of stem cell markers (SOX2, OCT-4, CD133) and impaired tumor-forming ability in nude mouse models. Furthermore, at the mechanistic level, it was determined that XPC overexpression is closely associated with reduced JAK2/STAT3 phosphorylation levels and attenuated stem cell properties, suggesting that XPC may influence lung cancer stem cell characteristics by regulating the JAK2/STAT3 signaling pathway. This association provides new insights into the link between DNA repair capacity and cancer stem cell properties. These findings establish XPC as a dual-function regulator that can both inhibit the maintenance of lung cancer stem cells and enhance the efficacy of chemotherapy, providing a promising therapeutic target for overcoming drug resistance in NSCLC.

Materials and methods

Cell culture. The human lung cancer cell line A549 (cat. no. TCHu150) and H460 (cat. no. TCHu205) were provided by the National Collection of Authenticated Cell Cultures. All cells were cultured in Dulbecco's modified Eagle's medium (DMEM; Pricella; Elabscience Bionovation Inc.; cat. no. PM150210) with 10% fetal bovine serum (FBS; Shanghai ExCell Biology, Inc.; cat. no. FSP500) and 1% penicillin-streptomycin (PS; Beijing Solarbio Science & Technology Co., Ltd.; cat. no. P1400) in a 5% CO_2 incubator at 37˚C. The two cell lines were certified as mycoplasma-free by the supplier upon receipt. During cell culture, mycoplasma contamination was routinely monitored using PCR-based detection methods, and no contamination was detected throughout the present study.

Reverse transcription-quantitative (RT-q) PCR. Total RNA was extracted from $1x10^6$ cells using the Super FastPure Cell RNA Isolation Kit (cat. no. RC102-01; Vazyme Biotech Co., Ltd.) according to the instructions in the manual.

RNA samples were removed from -80˚C and thawed at 4˚C. The reverse transcription reaction mixture was prepared according to the instructions for the ReverTra Ace qPCR RT Kit (cat. no. FSQ-101; Toyobo Co., Ltd.). After mixing all samples, the reverse transcription reaction was incubated at 37˚C for 15 min, followed by inactivation of the reverse transcriptase by incubation at 98˚C for 5 min.

qPCR amplification was performed using the cDNA obtained from reverse transcription as a template. The reaction system used SYBR Green PCR Master Mix (cat. no. A57156, Applied Biosystems; Thermo Fisher Scientific, Inc.) and detection was performed on the QuantStudio 3 Real-Time Fluorescent Quantitative PCR System (Applied Biosystems; Thermo Fisher Scientific, Inc.). The forward primer sequence for the XPC gene was 5'-CTTCGGAGGGCGATGAAA C-3' and the reverse primer sequence was 5'-TTGAGAGGT AGTAGGTGTCCAC-3'; The forward primer sequence for the internal control gene GAPDH was 5'-GGAGCGAGA TCCCTCCAAAAT-3', and the reverse primer sequence was 5'-GGCTGTTGTCATACTTCTCATGG-3'. The thermal cycling conditions were: An initial pre-denaturation step at 95˚C for 2 min, followed by 40 cycles, each consisting of 15 sec of denaturation at 95˚C and 60 sec of annealing at 60˚C. After the program ended, the Cq values for each group were recorded, and quantitative analysis was performed using the $2^{-\Delta\Delta Cq}$ method (31).

Animals. In the present study, 10 BALB/c-nu athymic nude mice (18-20 g, 6-week-old) were purchased from Jinan Pengyue Animal Breeding Co., Ltd [License No. SCXK (Lu) 2022 0006].

The animals were housed in the SPF-grade animal facility at the Experimental Animal Center of Weifang Second People's Hospital, with the temperature maintained at 20-26˚C and relative humidity stabilized at 40-70%. This temperature and humidity range aligns with the physiological requirements of nude mice, facilitating their metabolism and physiological functions while preventing health issues caused by inappropriate temperature and humidity conditions. The lighting used a system that simulates natural circadian rhythms, providing a 12-h light/dark cycle. The ventilation system was efficient, with air rigorously filtered to meet SPF-grade standards, effectively removing dust, microorganisms, and harmful gases. The air exchange rate was 10-20 times per h, ensuring fresh and high-quality air to safeguard the respiratory health

of experimental animals. The feed consisted of irradiated, SPF-grade experimental animal feed, and drinking water was supplied via a purified, sterile water system, which was provided to nude mice after high-pressure sterilization. The present study was approved by the Experimental Animal Ethics Committee of Weifang No.2 People's Hospital (approval no. 2024LAC019).

Bioinformatics analysis. The bioinformatics data came from clinical data on patients with lung adenocarcinoma patients in The Cancer Genome Atlas (TCGA) database and samples collected from unaffected tissue sites in the Genotype-Tissue Expression (GTEx) database, both date were from the UCSC Xena project (xena.ucsc.edu). Gene Expression Profiling Interactive Analysis (GEPIA; gepia.cancer-pku.cn) was used for data visualization.

Lentiviral transfection and efficiency detection. Stable cell lines with high XPC expression were constructed via lentiviral transfection. XPC-overexpressing lentivirus (gene ID: NM_004628, with GFP and puromycin resistance) and control lentivirus were purchased from WZ Biosciences Inc (Cat. no. CH894514). For transduction, lentivirus was added to A549 and H460 cells at a multiplicity of infection (MOI) of 10. The culture plates were incubated at 37˚C in a humidified environment containing 5% CO_2 for 24 h. Afterward, the virus-containing medium was removed and replaced it with fresh complete growth medium to minimize cytotoxicity. Purinomycin screening begins 48 h after transduction, with a final concentration of 1.0 μg/ml for A549 cells and 1.0 μg/ml for H460 cells; The screening medium was changed every two days, and untransduced cells maintained in parallel at the same puromycin concentration served as negative controls to confirm that uninfected cells had been completely eliminated. The screening process continued for 10 to 14 days, until all cells in the negative control wells had shed and died.

Western blotting. Protein was extracted using RIPA lysis buffer (Beyotime Biotechnology; cat. no P0013C). The BCA standard curve was determined using Pierce BCA Protein Assay Kits from Thermo Fisher Scientific, Inc. The protein (10 μg per lane) was separated using the Future PAGE 4-20% Protein Prep Gel (ACE Biotechnology Co., Ltd.; cat. no ET15420LGel) and transferred to a nitrocellulose membrane. After blocking with 5% skimmed milk powder for 1 h at room temperature, the membrane was incubated with the primary antibodies at 4˚C overnight. Following primary antibody incubation, the membranes were incubated with the secondary antibody for 1 h at room temperature. The proteins were visualized using an imaging system after immersion in ECL luminescent solution (Beyotime Biotechnology; cat. no P0018AM) for 2-3 sec. Semi-quantitative analyses were performed by ImageJ version 1.53t (National Institutes of Health).

Antibodies. The following primary antibodies were used in the present study: GAPDH mouse monoclonal antibody (cat. no. AB181602; 1:5,000), XPC rabbit monoclonal antibody (cat. no. AB309129; 1:1,000), SOX2 rabbit monoclonal antibody (cat. no. AB92494; 1:1,000), JAK2 rabbit monoclonal antibody (cat. no. AB108596; 1:1,000), phosphorylated (p-) JAK2 rabbit monoclonal antibody (cat. no. AB32101; 1:1,000), and p-STAT3 rabbit monoclonal antibody (cat. no. AB76315; 1:1,000) were purchased from Abcam (Shanghai) Trading Co., Ltd. STAT3 rabbit monoclonal antibody (cat. no. 4904S; 1:1,000) was purchased from Cell Signaling Technology (Shanghai) Biological Reagents Co., Ltd.

The following secondary antibodies were used in the present study: HRP-conjugated Goat Anti-Rabbit IgG(H+L) (cat. no. SA00001-2; 1:5,000), HRP-conjugated Goat Anti-Mouse IgG(H+L) (cat. no. SA00001-1; 1:5,000) was purchased from Proteintech (Wuhan) Group, Inc.

Cell-based immunofluorescence assay. Cells ($5x10^4$) were grown on glass coverslips and harvested after 24 h of culture. Following fixation with 4% paraformaldehyde (15 min, room temperature) and permeabilization with 0.1% Triton X-100 at room temperature, non-specific sites were blocked with 5% donkey serum (Mei5bio; cat. no MF835-01). Samples were incubated with the primary antibody (1:100 dilution) overnight at 4°C, washed three times with PBST (10 min each, room temperature), and then incubated with the AF555-conjugated secondary antibody (1:100 dilution) at room temperature for 60 min. After another three washes with PBST (10 min each, room temperature), the cell nuclei were counterstained with DAPI for 15 min at room temperature. Images were observed and collected using a fluorescence inverted microscope (20x objective lens), and were analyzed and quantified using ImageJ version 1.53t.

Cell proliferation and migration assay.

Cell growth curves. Cells in the logarithmic growth phase were seeded at a density of $2x10^4$ cells into a 24-well plate. After plating the cells were cultured in a 37˚C, 5% CO_2 incubator. Each day, a sample was taken from one group of cells, which were digested and centrifuged (800 x g; 5 min at room temperature.), then resuspend in PBS. The cells were then counted and the cell counts at each time point were recorded, a growth curve was plotted with time on the x-axis and cell count on the y-axis and the differences in cell proliferation between the two groups were compared.

Wound healing assay. To minimize the interference of cell proliferation on wound healing, scratch wound healing assays were conducted under serum-free conditions. Cells were grown to 90% confluence, and wounds were created using a sterile 200 μl pipette tip. After washing with PBS to remove detached cells, the medium was replaced with serum-free DMEM. Images of the wound area were taken at 0 and 24 h using an inverted microscope. The wound closure rate was calculated using the following formula:

$$[(\text{area at 0 h} - \text{area at 24 h}) / \text{area at 0 h}] \times 100\%.$$

Transwell migration. Cell migration assays were performed using 24-well Transwell chambers made from polycarbonate membranes with a pore size of 8.0 μm. A total of $2x10^4$ cells in 200 μl of serum-free DMEM were seeded into the upper chamber, while 600 μl of DMEM containing 10% FBS (as a chemotactic factor) was added to the lower chamber. After incubation for 24 h in a humidified incubator at 37˚C and 5% CO_2, uninvaded cells on the upper surface were gently

removed with a cotton swab. Cells that had migrated through the Transwell and adhered to the bottom were fixed with 4% formaldehyde for 15 min at room temperature, followed by staining with DAPI for 20 min at room temperature. Images of the invading cells were captured at 200x magnification using a fluorescence inverted microscope and five random fields of view were selected from each membrane for counting. Each experiment was repeated three times.

Colony formation. A total of $1x10^3$ cells were grown in the logarithmic growth phase into a 60-mm culture dish, incubated in a 37˚C, 5% CO_2 incubator, the medium changed every 3 days. The medium was discarded after 14 days, washed three times with PBS, stained with crystal violet for 30 min at room temperature and finally washed 2-3 times with PBS. The plate was then imaged and the colonies (≥0.5 mm in diameter) were counted.

Drug sensitivity testing. The MTS assay was used to detect cell viability after treating cells with different concentrations of drugs and the IC_{50} value was calculated to determine the sensitivity of cells to the drug. After adding the cells into in a 96-well plate and incubating for 24 h, the model drug [doxorubicin (DOX) or cisplatin (CDDP)] was diluted in a 2-fold gradient at a maximum concentration of 6 μg/ml or 100 μg/ml, respectively. After 72 h, MTS was used to detect different cell activities, and GraphPad 8 software (Dotmatics) was used to fit the IC_{50} curve of the cells. Subsequently, cell activity was measured at 24 and 48 h, with the IC_{50} value as the intermediate point.

Cell viability (%)=(OD test-OD blank)/(OD control−OD blank) x 100%

Apoptosis assay. Cells were seeded at a density of $2x10^5$ cells per well in a 6-well plate and treated with CDDP for 72 h. Apoptosis was detected using the Annexin V-YSFluor™ 647/7-AAD Apoptosis Detection Kit (Shanghai Yeasen Biotechnology Co., Ltd.; cat. no. 40312ES60) according to the manufacturer's instructions. Briefly the steps were as follows: The cells were harvested, washed with cold PBS and resuspend in 1X binding buffer. Annexin V-YSFluor™ 647 and 7-AAD, were added and incubated for 15 min at room temperature in the dark. Flow cytometric analysis was performed using the RaiseCyte2L6C flow cytometer and the data was analyzed using FlowJo software (v 10.8.1l BD Biosciences), and early apoptotic cells (Annexin V^+/7-AAD^-) and late apoptotic/necrotic cells (Annexin V^+/7-AAD^+) were quantified.

DNA damage detection (TUNEL assay). DNA damage was assessed using a TUNEL assay kit (Beyotime Biotechnology; cat. no. C1090). Cells were treated with CDDP for 72 h, fixed with 4% glutaraldehyde, permeabilized with 0.3% Tween X-100, and incubated with the TUNEL reaction mixture at 37˚C for 60 min. Images were captured under a fluorescence microscope, and TUNEL-positive cells were quantified using ImageJ version 1.53t (National Institutes of Health).

Drug accumulation. Cells were seeded at a density of $3x10^4$ cells into a 24-well plate and were treated with 10 μg/ml DOX for 2, 4 and 6 h. After washing three times with ice-cold PBS, the cells were fixed with 4% paraformaldehyde for 15 min at room temperature. DOX fluorescence was observed using an inverted fluorescence microscope and quantitative analysis of the average fluorescence intensity at each time point was performed using ImageJ version 1.53t (National Institutes of Health).

Sphere assay. Sphere assay were performed using AggreWell™ 400 (STEMCELL Technologies; cat. no.: 34411). Each well was seeded with $1x10^3$ cells and cultured in serum-free DMEM medium containing B27 (1X), EGF (20 ng/ml), and bFGF (20 ng/ml). The medium was changed every 2 days. At the end of the culture period, images were captured and the number of spheroids with a diameter ≥50 μm was counted to assess the cells ability of the cells to grow in suspension and their self-renewal capacity.

Observation of tumor proliferation capacity in vivo. The present study was conducted using 6-week-old, male, nude mice, all of which were male, weighing 18-20 g. The mice were randomly divided into two groups, with five mice in each group. A549-CTR and A549-XPC cells in the logarithmic growth phase were diluted to $1x10^7$ cells/ml using DMEM medium containing 1% FBS. Tumor cells were stored on ice. and 200 μl of the cell suspension ($2x10^6$ cells/mice) was injected subcutaneously into the dorsal aspect of the left hind limb of the nude mice using a 1 ml syringe, labeled as the A549-CTR group and A549-XPC group. After 5 min of rest, the injection site was disinfected with a sterile cotton swab dipped in 75% alcohol.

After establishing the xenograft tumor model, the physiological status and tumor growth of the nude mice were observed daily. Once the tumor was visible to the naked eye (longest diameter >2 mm), the longest and shortest sides of the subcutaneous tumor were measured every 2 days using a Vernier caliper, denoted as L_a and L_b, respectively. Tumor volume was calculated using the following formula: $V=L_a \times L_b^2/2$, where V denotes tumor volume; L_a, tumor long axis; and L_b, tumor short axis.

After 12 measurements were taken, the nude mice were sacrificed using carbon dioxide asphyxiation (carbon dioxide was injected into the euthanasia device at a volume replacement rate of 30%/min). The tumor tissue was collected for image capture and weighing and the excised tumor tissue was stored in 4% paraformaldehyde. In the subcutaneous tumor implantation experiments with nude mice conducted in this study, the following humane endpoints were established: The diameter of the tumor in any dimension must not exceed 15 mm (maximum diameter 11.04 mm), the tumor volume must not exceed 2,000 mm^3 (maximum volume 452.10 mm^3), and the tumor weight must not exceed 10% of the animal's body weight. During the experiment, the animals' body weight and tumor growth were monitored daily; when any of these parameters reached the aforementioned thresholds, the experimental animals were immediately sacrificed. No animals reached the aforementioned thresholds.

Statistical analysis. To compare the means of two independent samples, unpaired independent-samples t-test were employed. This test is suitable for determining whether there is a

statistically significant difference between the means of two groups. For comparisons involving multiple groups, one-way analysis of variance (ANOVA) was used to detect significant differences among the means of multiple groups and Tukey's multiple comparisons test was used for post hoc tests. For longitudinal tumor volume data collected at multiple time points from the same group of animals and longitudinal drug uptake data collected at multiple time points from the same group of cells, a two-factor repeated-measures ANOVA was performed, with time as a within-group factor and different cell types as a between-group factor. In the post hoc analysis, the Sidak multiple comparison test was used to perform pairwise comparisons between groups at each time point. For survival analysis, Kaplan-Meier survival curves were plotted using JASP 0.98.1, and the log-rank test was used to assess differences in survival rates among groups. All quantitative data are presented as mean ± standard deviation (SD) unless otherwise stated. $P<0.05$ was considered to indicate a statistically significant difference. Statistical analyses were performed using GraphPad Prism 8.0.2 (Dotmatics).

Results

XPC suppresses proliferation and metastasis of NSCLC. First the transcription level of XPC was analyzed in lung cancer tissues from the TCGA database using the GEPIA platform. The results showed that XPC expression was decreased in human LUAD tissues (Fig. 1A; $P<0.001$). Furthermore, survival analysis of lung cancer patients with different XPC expression levels via the Kmplot platform (https://kmplot.com/analysis/) showed that the median survival of patients with low XPC expression was 52 months, which was only 61.90% of that in patients with high XPC expression. This exploratory bioinformatics analysis suggests a possible association between reduced XPC expression and poor survival prognosis (Fig. 1B; $P<0.001$).

To investigate the functional effect of XPC expression levels in tumors, the present study established two XPC-overexpressing cell lines, A549-XPC and H460-XPC, using lentiviral transduction. RT-qPCR results showed that the XPC transcript level in A549-XPC cells was 10.75 times higher than in A549-CTR cells (H460-XPC vs. H460-CTR, 8.76 times; Fig. S1A; $P<0.01$). Furthermore, western blotting confirmed that the XPC protein level in A549-XPC cells was 3.90 times that of the control group (H460-XPC vs. H460-CTR, 4.35 times; Fig. 1C and D; $P<0.001$). Additionally, immunofluorescence assays indicated that the overexpressed XPC was primarily localized in the nucleus, which is consistent with previously reported expression patterns of XPC (Fig. S1B and C) (32). These results confirmed the successful establishment of the two XPC-overexpressing cell lines, A549-XPC and H460-XPC and their control lines, which can be used to study the functional differences mediated by XPC in tumor cells.

The growth curves of the different cell lines during cell culture were recorded. Within the recording period, the control groups entered the exponential growth phase by day 2, whereas the XPC-overexpressing groups did not enter the exponential growth phase even by day 4. At day 4, the cell number in the control groups was significantly higher than in the experimental groups, suggesting that XPC overexpression inhibits the proliferation of tumor cells (Fig. 1E; $P<0.001$). The *in vitro* cell colony formation assay further supported the view that XPC overexpression inhibits tumor cell proliferation ability (Fig. 1F and G; $P<0.001$; Fig. S2A and B). The number of cell colonies formed by XPC-overexpressing cells was only 65.31% of that in the control groups.

Migration is a crucial capability for tumor cell metastasis; therefore, the effect of XPC overexpression on tumor cell migration was investigated. The scratch wound healing assay showed that the wound closure in the experimental cell lines after 24 h of culture was significantly lower than in the control groups. The wound healing capacity was reduced by 0.77-fold compared with the control groups (Fig. 1H-J; $P<0.001$; Fig. S3A and B). Furthermore, the invasive capability of the cells was assessed using the Transwell assay. As expected, fewer A549-XPC cells migrated through the membrane in the same amount of time (Fig. 1I-K; $P<0.001$; Fig. S3C and D). Subsequently, the tumor cells were labeled with PE and analyzed the cell cycle of the different groups using flow cytometry. The results showed a significant reduction in the proportion of cells in the G_2/M phase in the XPC-overexpressing groups (Fig. 1L and M; $P<0.05$; Fig. 2C and D), suggesting that XPC inhibits tumor cell proliferation by reinforcing the G_2/M checkpoint. These results indicated that reduced expression of XPC in tumor cells enhanced their proliferation and migration capabilities, leading to increased tumor malignancy, and that XPC is a key negative regulator of NSCLC growth and metastasis.

Mechanisms of XPC-mediated modulation of sensitivity to CDDP and DOX in lung cancer cells. CDDP and DOX are front-line cytotoxic agents against NSCLC and their primary mode of action is the induction of DNA damage. XPC, the key sensor of helix-distorting adducts, initiates global-genome nucleotide excision repair. It was therefore hypothesized that elevated XPC could potentiate the lethal effects of these drugs.

Indeed, 72 h exposure to either CDDP or DOX yielded markedly lower half-maximal inhibitory concentrations (IC_{50}) in XPC-over-expressing cell sub-lines compared with empty-vector controls (Fig. 2A and B and Fig. S4A and B). Subsequent time- and dose-response profiling revealed that cytotoxicity increased in a strictly concentration- and schedule-dependent manner for both agents (Fig. 2C-H and Fig. S4C-F). Notably, at every concentration and time point examined, XPC-high cells exhibited consistently greater sensitivity to CDDP or DOX than their XPC-low counterparts.

To elucidate the mechanism underlying XPC-mediated chemotherapy sensitization, the present study assessed cell apoptosis, DNA damage burden and drug accumulation. Analysis of the time course of DOX accumulation revealed that, compared with the control group, A549-XPC cells exhibited significantly elevated intracellular fluorescence intensity (relating to DOX uptake) at 2, 4 and 6 h, with the most significant difference observed at 4 h (Fig. 2I-K; $P<0.01$). Following treatment with cisplatin, the apoptosis rate in XPC-overexpressing cells was significantly higher compared to the control group (Fig. 2L and M; $P<0.01$). TUNEL staining revealed significantly increased DNA damage in XPC-overexpressing cells following drug exposure (Fig. 2N and O; $P<0.01$). These

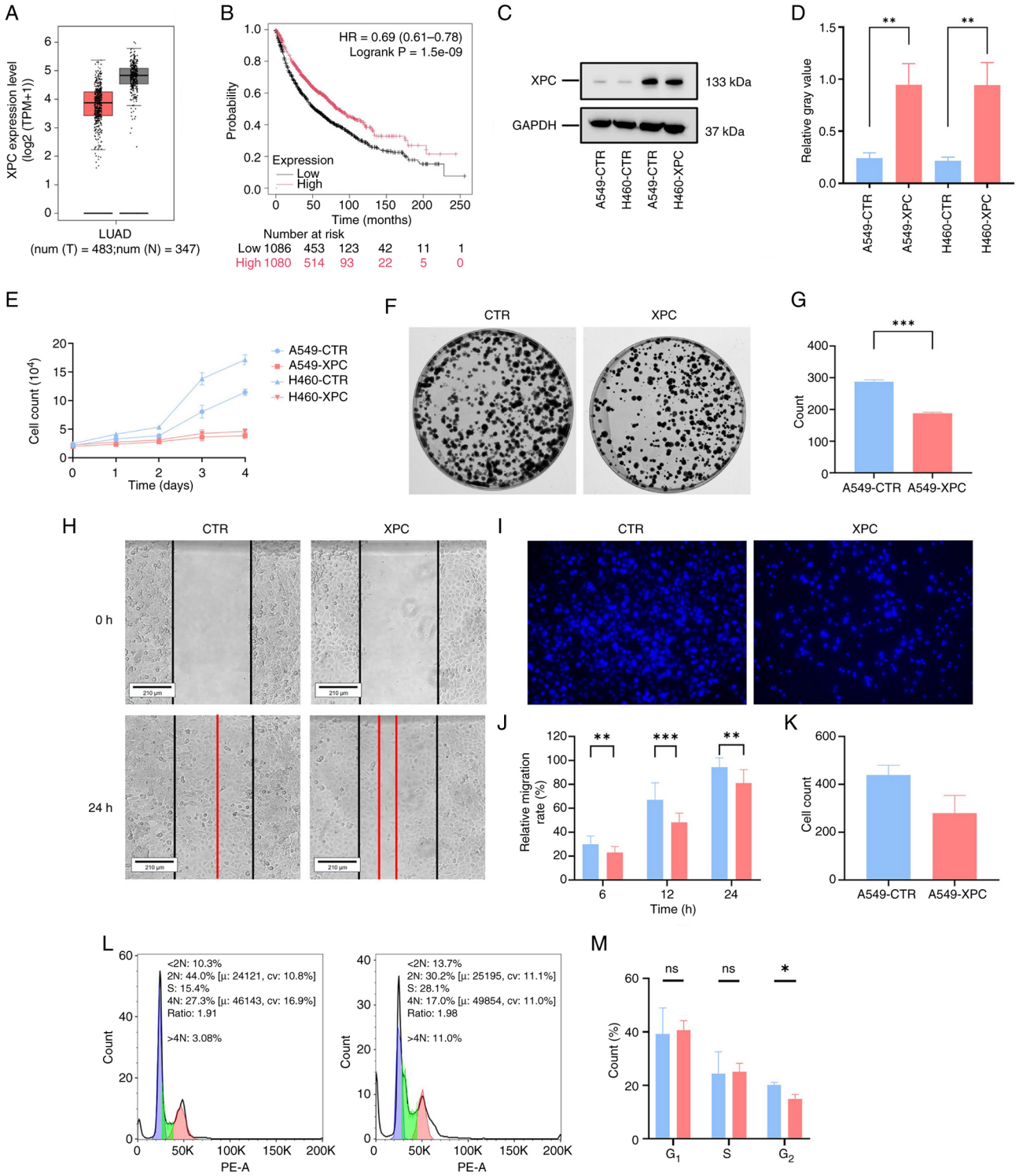

Figure 1. XPC inhibits cell proliferation, migration and induces cell cycle arrest in non-small cell lung cancer. (A) Analysis of XPC transcript levels in lung adenocarcinoma tissues from TCGA database using GEPIA. (B) Survival analysis of lung cancer patients with different XPC expression levels via Km-plot platform. (C) Western blotting of XPC protein expression in XPC-overexpressing cell lines. (D) Quantitative analysis of western blotting results. (E) Cell growth curves (n=3). (F) Representative images of cell colony formation assay. (G) Quantitative analysis of colony formation (n=3). (H) Representative images of scratch wound healing assay (scale bar, 200μm), the red line indicates the cell boundary at the end of the experiment. (I) Representative images of Transwell cell migration assay (scale bar, 100 μm). (J) Quantitative analysis of wound healing rate (n=3). (K) Quantitative analysis of cell migration in Transwell assay (n=3). (L) Cell cycle distribution analyzed by flow cytometry. (M) Quantitative analysis of cell cycle phase proportions (n=3). All data are presented as mean ± SD. *P<0.05, **P<0.01, ***P<0.001; ns, no significant difference. XPC, xeroderma pigmentosum group C; TCGA, The Cancer Genome Atlas; GEPIA, Gene Expression Profiling Interactive Analysis; LUAD, lung adenocarcinoma; HR, Hazard Ratio; CTR, control.

data suggested that XPC-mediated chemotherapy sensitivity involves enhanced apoptosis induction, an increased DNA damage burden, and elevated intracellular drug accumulation.

XPC-regulated expression of stemness-associated markers and JAK/STAT signaling in lung cancer cells. To determine whether XPC abundance modulated the stem-like properties

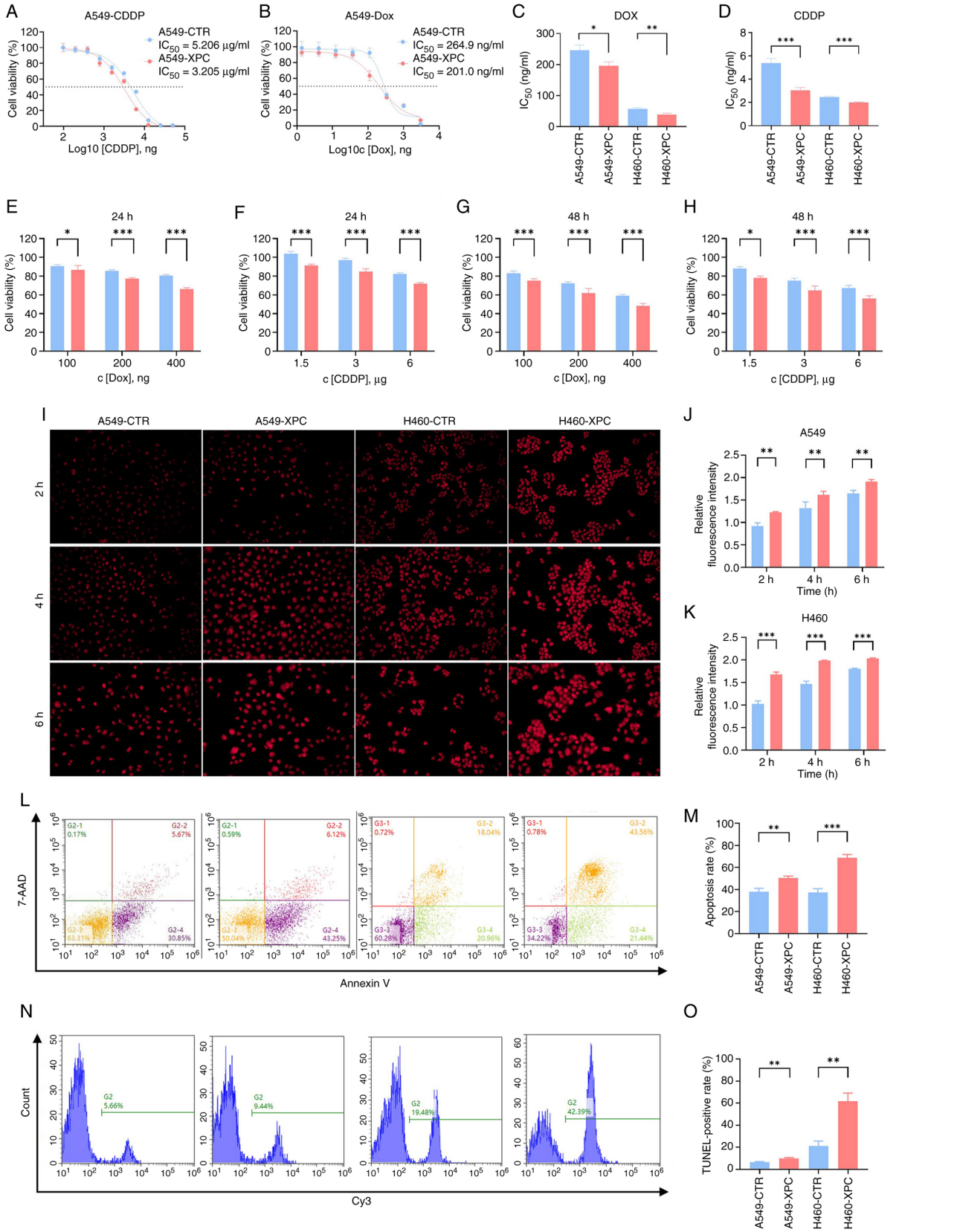

Figure 2. High XPC expression affects drug resistance in different cell lines. IC_{50} of A549 cells for (A) CDDP and (B) DOX. (C-D) Statistical analysis of IC_{50} values among different drug treatment groups. The analysis of cell viability and IC_{50} values after treatment with DOX for (E) 24 h or (G) 48 h in A549 cells; and CDDP for (F) 24 h or (H) 48 h in A549 cells. (I) Representative immunofluorescence images showing intracellular DOX accumulation in A549-CTR, A549-XPC, H460-CTR and H460-XPC cells 2, 4 and 6 h after treatment with 10 μg/ml DOX. Objective magnification is 20x. Quantitative analysis of the relative fluorescence intensity of DOX accumulation in (J) A549 and (K) H460 cells at specified time points. (L) Representative flow cytometry profiles showing apoptosis detected by Annexin V-YSFluor 647/7-AAD staining in the specified cell lines 72 h after CDDP treatment. (M) Quantitative analysis of the apoptosis rate in the specified cell lines. (N) Representative flow cytometry histogram showing TUNEL-positive cells in the specified cell lines 72 h after CDDP treatment. (O) Quantitative analysis of the TUNEL-positive cell percentage in the specified cell lines. *P<0.05, **P<0.01, ***P<0.001. XPC, xeroderma pigmentosum group C; CDDP, cisplatin; DOX, doxorubicin; CTR, control.

of NSCLC cells, the expression of SOX2 (34 kDa) was first examined. Western blotting revealed a pronounced reduction in SOX2 protein in XPC-overexpressing cell sub-lines relative to vector controls (Fig. 3A and B and Fig. S5A and B), suggesting altered expression of stemness-associated markers and flow-cytometric analyses corroborated this finding: OCT-4 levels were markedly lower, and the $CD133^+$ fraction was significantly decreased in XPC-high cell populations ($P<0.01$; Fig. 3C and D and Fig. S5C and D). Collectively, these data indicated that enforced XPC expression reduces the expression of stemness-associated markers (SOX2, OCT-4 and CD133) in NSCLC cells.

Mechanistically, interrogation of the JAK/STAT axis showed that XPC overexpression selectively impaired pathway activity: p-JAK2 and p-STAT3 were both substantially reduced, without a concomitant decline in total STAT3 (Fig. 3G-I). Surprisingly, total JAK2 protein was markedly elevated, suggesting a compensatory feedback loop that attempts to restore signaling capacity in the face of persistent p-JAK2 attenuation. Thus, XPC reduces SOX2-driven stemness, at least in part, by dampening JAK/STAT3 signaling in NSCLC cells.

Effects of XPC on clonogenic ability and serum-dependent growth of lung cancer cells. To quantitatively assess the effect of XPC on tumor initiation capacity, a spheroid formation assay was conducted in serum-free, ultra-low-adhesion 24-well round-bottom plates (Fig. 4). A total of 8 days after seeding, the spheroids formed by A549-XPC cells were markedly smaller than those in the A549-CTR control group, and their spheroid formation efficiency was also markedly lower than that of the A549-CTR control group. The same trend was observed in H460 cells, confirming that elevated XPC levels inhibit the self-renewal capacity of NSCLC cells with different genetic backgrounds.

Roles of XPC in tumorigenesis and tumor growth characteristics. Tumor growth was analyzed using two-way repeated-measures ANOVA, which revealed a significant main effect of XPC overexpression on tumor volume over time (Fig. 5; $P<0.05$). A549-XPC lesions grew slower than the controls, yielding markedly smaller volumes from day 9 onward, the final measurement taken on day 24 showed that the tumor volume (134.04 ± 46.77 mm^3) in the A549-XPC group was 41.28% of that in the control group (324.64 ± 85.31 mm^3), representing a significant reduction. At the endpoint, the excised tumors were weighed. The mean mass in the XPC-overexpression group (164.24 ± 76.16 mg) was 62% lower than the control (434.70 ± 115.72 mg). These data demonstrated that elevated XPC suppresses the *in vivo* tumorigenic potential of A549 cells.

In the tissues with immunofluorescence staining, the expression levels of tumor stem cell markers such as CD133, OCT4 and SOX2 were detected in different tissues (Fig. 6 and Fig. S6). The results showed that the expression levels of these markers were markedly reduced in tumor tissues with overexpressed XPC. Additionally, the proliferative activity of tumor tissues was demonstrated through Ki-67 staining, and the results showed a significant decrease in Ki-67 expression levels in tumor tissues with high XPC expression. This result illustrated the inhibitory effect of XPC on the stemness and proliferative capacity of malignant tumor cells.

Discussion

XPC is the primary sensor of DNA adducts and initiates genome-wide nucleotide excision repair (33-37). The present study investigated the role of XPC mRNA expression levels as a potential prognostic marker for treatment outcomes in NSCLC cell lines; while bioinformatic analyses of patient datasets have suggested associations, these associations still need to be validated in prospective studies. Our previous study found that downregulating XPC in tumor cells via shRNA leads to enhanced tumor stemness and upregulation of related molecular markers (15). It was hypothesized that XPC may exert its anti-tumorigenic, anti-invasive and anti-metastatic effects, as well as improve the prognosis of lung adenocarcinoma patients, by regulating the stemness of lung cancer cells. However, the specific mechanisms underlying these effects require further investigation.

The present study established A549 and H460 NSCLC cell lines overexpressing XPC using lentiviral transfection and assessed XPC expression at the mRNA and protein levels. Functional assays demonstrated that XPC overexpression inhibits cell proliferation, migration and clonogenic capacity, while enhancing sensitivity to CDDP and DOX. Mechanistically, cells with high XPC expression exhibited S-phase arrest, reduced SOX2 expression and attenuated JAK2/STAT3 phosphorylation. Notably, the present data indicated that overexpression of XPC enhanced cellular sensitivity to CDDP and DOX. The potential involvement of p53 in this sensitization effect was not examined in the present study and remains an important limitation to be addressed in future work. The present mechanistic studies have revealed the cause of this seemingly paradoxical phenomenon: Cells with high XPC expression exhibit enhanced drug-induced apoptosis, an increased DNA damage burden and elevated intracellular drug accumulation. This is consistent with the findings of certain studies, which suggest that under genotoxic conditions, the overactivation or dysregulation of DNA repair can exacerbate replicative stress and apoptotic signaling (38,39). *In vivo*, XPC overexpression markedly suppressed tumor formation in a subcutaneous xenograft model. The present findings indicated that elevated XPC expression suppressed lung cancer stem cell characteristics and enhanced sensitivity to CDDP and DOX chemotherapy. The increased sensitivity observed in XPC-overexpressing cells is associated with enhanced intracellular accumulation of DOX, suggesting that, in addition to its known role in DNA damage recognition, XPC may also promote drug uptake or retention. These elevated intracellular drug concentrations, combined with XPC-mediated initiation of DNA repair, likely enhance DNA damage-mediated cell death during genotoxic chemotherapy. Furthermore, XPC-mediated inhibition of the JAK2/STAT3 pathway and downregulation of stemness markers (SOX2, OCT-4 and CD133) may lower the drug resistance threshold by depleting the cancer stem cell pool, which inherently resists conventional chemotherapy (40,41).

In addition, the present study examined the activation status of the JAK/STAT pathway in NSCLC cells following XPC overexpression. The results showed that the phosphorylation

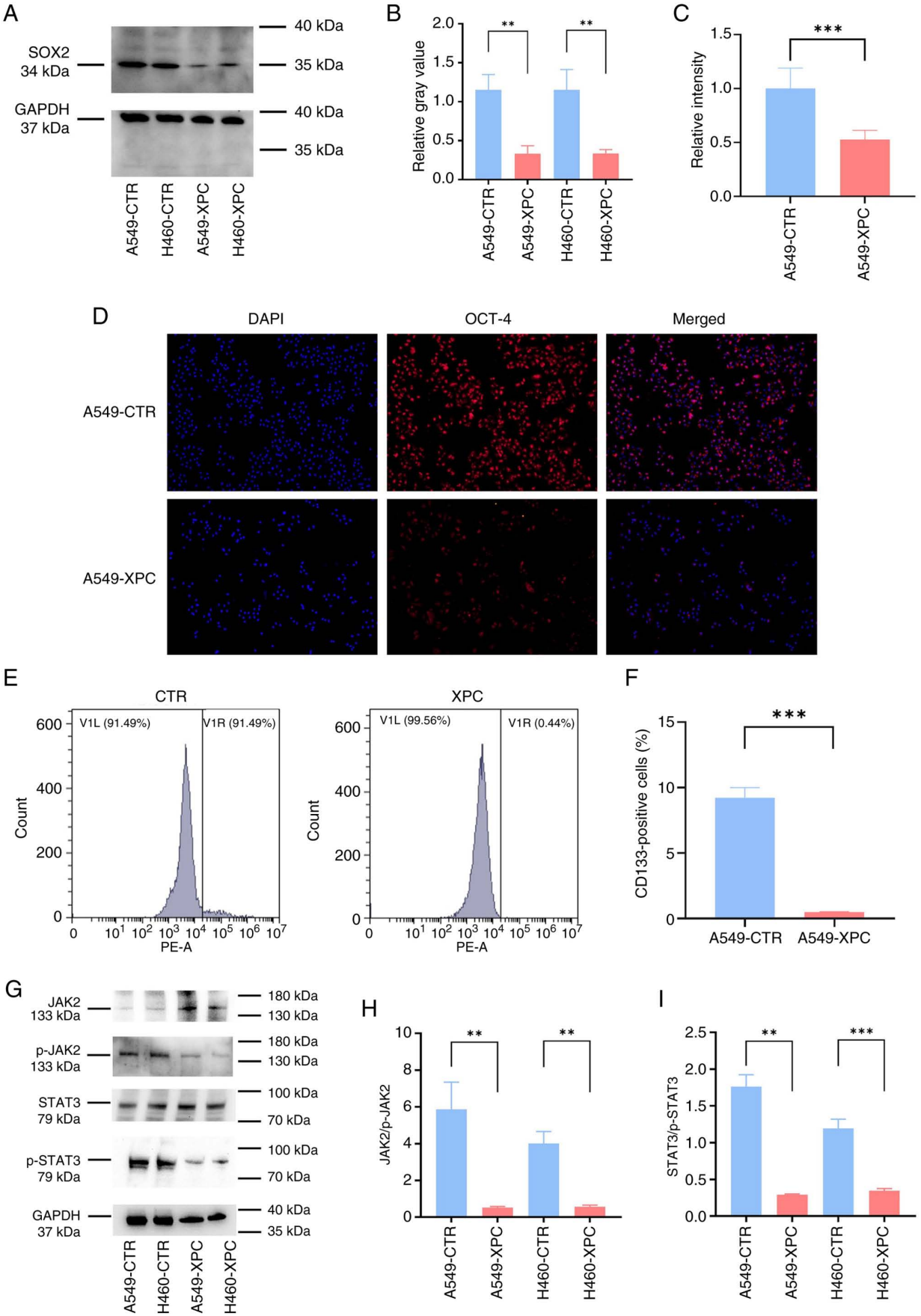

Figure 3. High expression of XPC is associated with reduced expression of tumor cell stemness markers and attenuated JAK/STAT signaling activation. (A) Western blotting of XPC expression in tumor cells. (B) Western blotting quantification results. (C) Quantitative results chart of cellular immune fluorescence assay. (D) Cellular immune fluorescence assay to detect XPC expression in tumor cells. Objective magnification is 10x. (E) Flow cytometry detection of XPC expression in tumor cells. (F) Quantification of flow cytometry results. (G) Western blotting of JAK2/STAT3 in tumor cells; (H and I) western blot quantification results. **P<0.01, ***P<0.001. XPC, xeroderma pigmentosum group C; CTR, control.

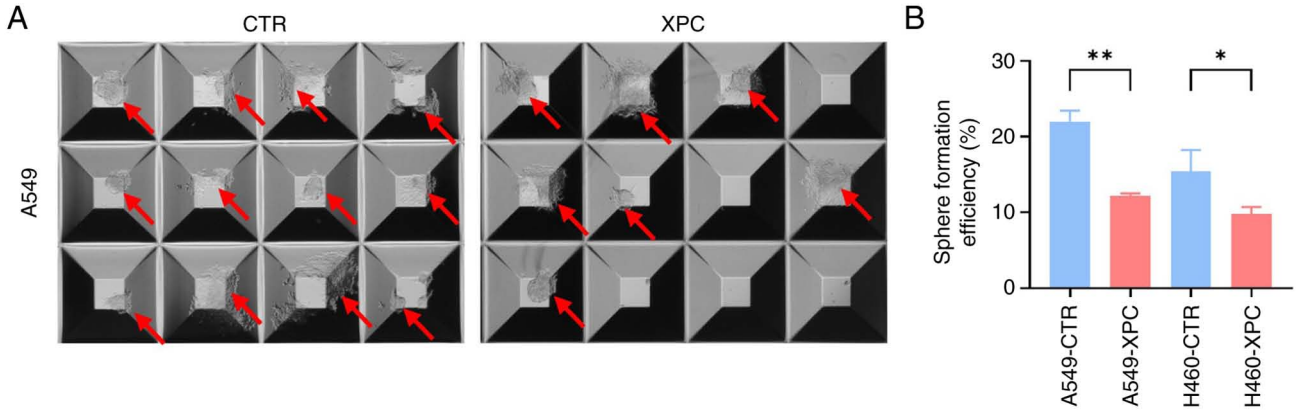

Figure 4. Reduced anchorage-independent spheroid formation in XPC high-expressing cells under serum-free conditions. (A) Image of cell spheroid formation (4x objective) and (B) quantitative analysis of the results. *P<0.05, **P<0.01. XPC, xeroderma pigmentosum group C; CTR, control.

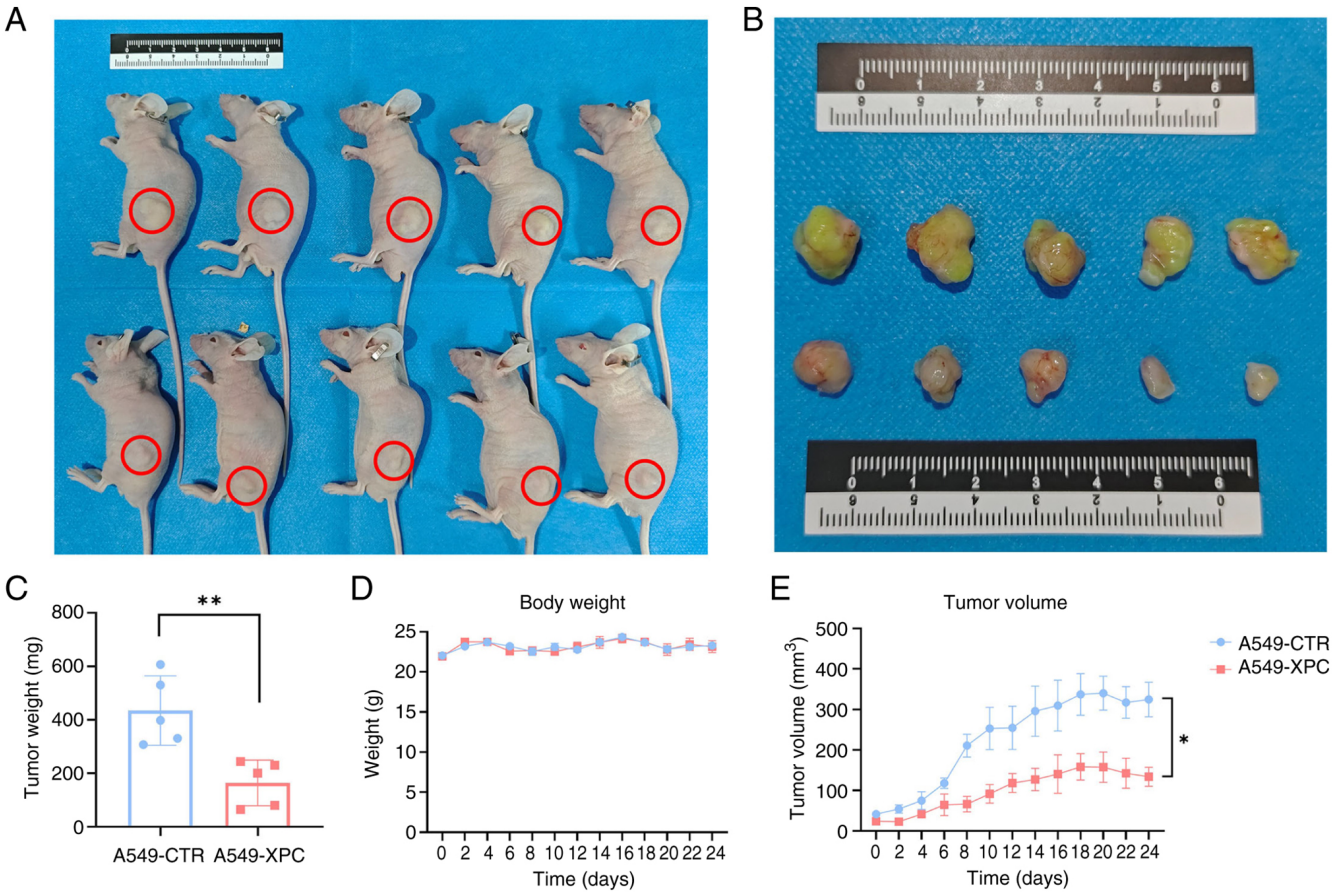

Figure 5. XPC overexpressing cells have reduced *in vivo* tumorigenicity. (A) Condition of nude mice 24 days after subcutaneous tumor implantation. (B) Tumor condition 24 days after subcutaneous tumor implantation. (C) Tumor weight 24 days after subcutaneous tumor implantation. (D) Line graph of body weight changes 24 days after subcutaneous tumor implantation. (E) Line graph of tumor volume changes 24 days after subcutaneous tumor implantation. *P<0.05, **P<0.01. XPC, xeroderma pigmentosum group C; CTR, control.

levels of the JAK2/STAT3 pathway were markedly reduced in cells with high XPC expression, concomitant with decreased SOX2 expression levels. Thus, regulating XPC expression levels within tumor cells may play a crucial role in mitigating the progression and drug resistance of NSCLC. These observations suggested that XPC may be associated with the modulation of JAK2/STAT3 signaling and participate in regulating lung cancer stemness; however, this association is currently associative and requires further mechanistic validation. Additionally, the role of p53 in XPC-mediated effects on chemotherapy sensitivity and stem cell characteristics was not investigated in the present study, representing a further limitation that should be explored in subsequent research.

These preclinical findings suggested that XPC expression may warrant further investigation in a clinical setting; however, any speculation regarding its role as a prognostic

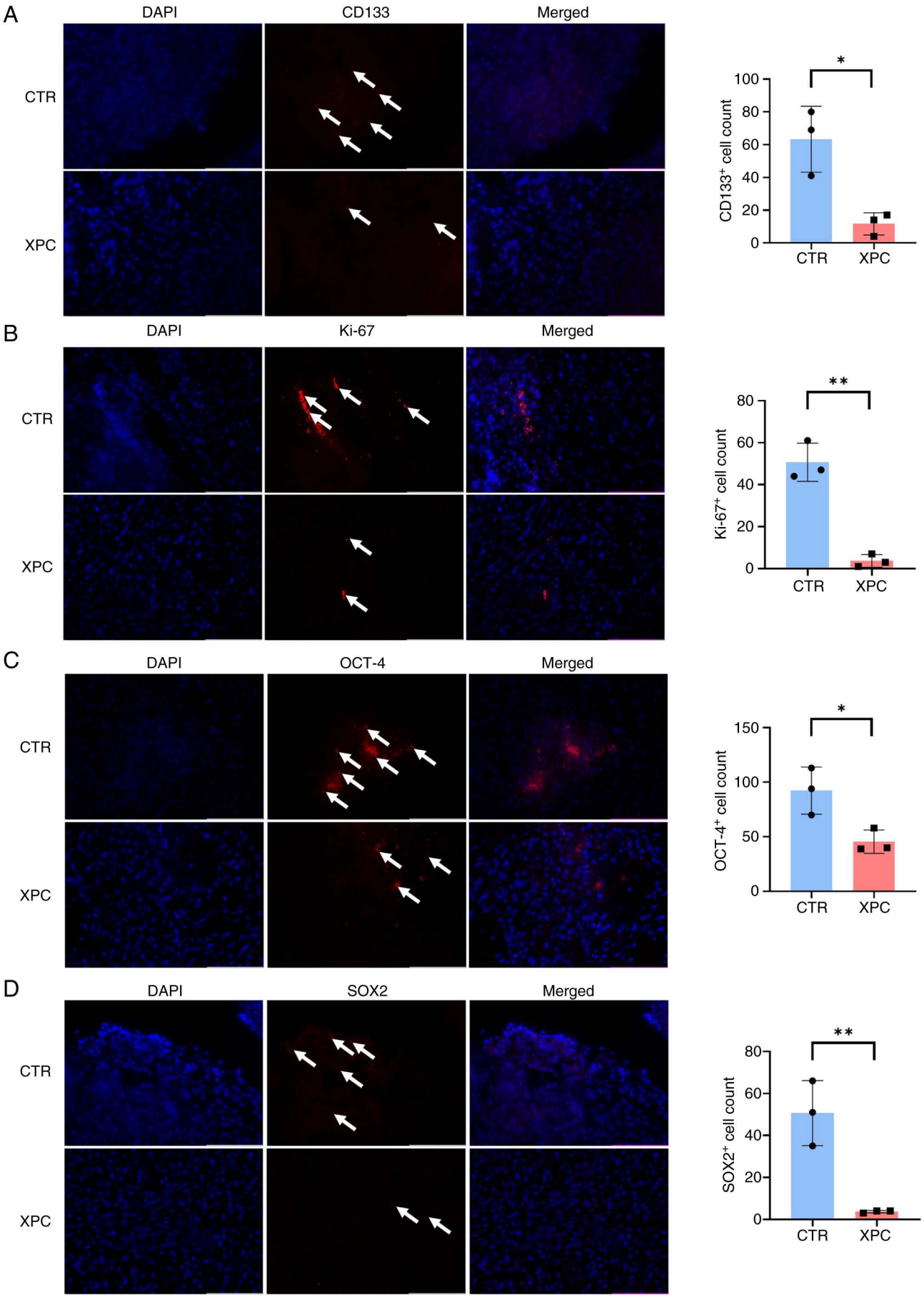

Figure 6. The stemness and proliferative activity of tumor cells with high expression of XPC are reduced. Cell immunofluorescence experiments show the cells and quantitative analysis of (A) CD133+ (B) Ki-67+ (C) OCT-4+ and (D) SOX2+ in tumor tissues (Objective magnification is 10x). The arrows indicate positive cells. *P<0.05, **P<0.01. XPC, xeroderma pigmentosum group C; CTR, control.

marker or therapeutic target is based on exploratory bioinformatics analyses and *in vitro*/*in vivo* models, and independent clinical or prospective cohort validation is required before such conclusions can be drawn. Based on current preclinical data, partially restoring XPC expression in tumors through pharmacological means may be a potential future strategy for overcoming chemotherapy resistance.

The present study had several limitations. Although the present study demonstrated the effect of highly expressed XPC on lung cancer stem cell characteristics and its association with inhibition of the JAK/STAT signaling pathway, a causal relationship between XPC and JAK2/STAT3-mediated regulation of lung cancer stemness remains to be established. In addition, the specific mechanisms by which XPC functions in DNA damage repair processes within lung cancer stem cells remain poorly understood. As a key protein in the NER pathway, the role of XPC in lung cancer stem cells may extend beyond the recognition and repair of DNA damage (42). Further research is needed to determine whether XPC regulates the characteristics of lung cancer stem cells by affecting specific DNA repair protein complexes and whether this regulation is associated with the inhibition of the JAK/STAT signaling pathway.

In conclusion, high expression of XPC in lung cancer cells is associated with reduced expression of stemness-associated markers (SOX2, OCT-4, CD133), decreased phosphorylation of JAK2 and STAT3 and attenuated stem cell-like characteristics. While these findings suggested a potential link between XPC and JAK2/STAT3-mediated regulation of lung cancer stemness, further mechanistic studies are required to establish causality. *In vitro* studies showed that high expression of XPC reduced the proliferation and migration capacity of lung cancer cells; *in vivo* studies indicated that high expression of XPC decreases the tumorigenic potential of tumor cells *in vivo*. Additionally, high XPC expression enhanced the sensitivity of lung cancer cells to DNA-damaging chemotherapeutic agents, improving the antitumor efficacy of drugs such as CDDP and DOX. Future studies should aim to further explore the molecular mechanisms of XPC in lung cancer development, potentially leading to the development of new tumor treatment strategies based on XPC.

Acknowledgements

Not applicable.

Funding

The present study was supported by the National Natural Science Foundation of China, (grant no. 81871892), the Weifang City Science and Technology Project Plan (grant nos. 2024JZ0018 and 2023YX077) and Weifang Municipal Health Commission Scientific Research Program (grant nos. WFWSJK-2022-008 and WFZYY2025-4-008).

Availability of data and materials

The data generated in the present study may be requested from the corresponding author.

Authors' contributions

MQ and SW performed conceptual design. BY conducted methodology and performed experiments. The data were quantified and analyzed by YY, WW and YbW. HW, LQ and YmW performed bioinformatics analyses. SS examined the physiological indicators of the animals. BY and YY supervised and participated in the cell experiments. BY, SW and MQ wrote the original manuscript. MQ and BY reviewed and edited the article, supervised by MQ. MQ was responsible for project management. SW and MQ confirm the authenticity of all the raw data. All authors read and approved the final manuscript.

Ethics approval and consent to participate

The present study has been approved by the Laboratory Animal Ethics Committee of Weifang Second People's Hospital (approval no. 2024LAC019).

Patient consent for publication

Not applicable.

Competing interests

The authors declare that they have no competing interests.

Use of artificial intelligence tools

During the preparation of this work artificial intelligence tools were used to improve the readability and language of the manuscript and subsequently the authors reviewed and edited the content produced by the artificial intelligence tools as necessary, taking full responsibility for the ultimate content of the publication.

References

1. Vaccaro A, Rahal Z, Kadara H and Cascone T: A roadmap to precision immunotherapy for early-stage non-small cell lung cancer. Cancer Discov 15: 884-889, 2025.
2. Qu T, Song L, Xu J, Lu X, Yin D, Dai J, Zhang C, Guo R and Zhang E: MYLK-AS1 enhances glutamine metabolism to promote EGFR inhibitor resistance in non-small cell lung cancer. Cancer Res 85: 3052-3071, 2025.
3. Kenmotsu H, Yamamoto N, Misumi T, Yoh K, Saito H, Sugawara S, Yamazaki K, Nakagawa K, Sugio K, Seto T, *et al*: Five-year overall survival analysis of the JIPANG study: Pemetrexed or vinorelbine plus cisplatin for resected stage II-IIIA nonsquamous non-small-cell lung cancer. J Clin Oncol 41: 5242-5246, 2023.
4. Guevara Lopez ML, Gebo A, Parodi M, Persano S, Maus-Conn J, Mingari MC, Loiacono F, Orecchia P, Sivori S, Cantoni C, *et al*: $CD56^{bright}$ cytokine-induced memory-like NK cells and NK-cell engagers synergize against non-small cell lung cancer cancer-stem cells. J Immunother Cancer 13: e010205, 2025.
5. Shi L, Li B, Tan J, Zhu L, Zhang S, Zhang Y, Xiang M, Li J, Chen Y, Han X, *et al*: Exosomal lncRNA Mir100hg from lung cancer stem cells activates H3K14 lactylation to enhance metastatic activity in non-stem lung cancer cells. J Nanobiotechnology 23: 156, 2025.
6. Testa U, Castelli G and Pelosi E: Lung cancers: Molecular characterization, clonal heterogeneity and evolution, and cancer stem cells. Cancers (Basel) 10: 248, 2018.
7. Zebian A, Shaito A, Mazurier F, Rezvani HR and Zibara K: XPC beyond nucleotide excision repair and skin cancers. Mutat Res Rev Mutat Res 782: 108286, 2019.

8. Lindsey-Boltz LA, Yang Y, Kose C, Deger N, Eynullazada K, Kawara H and Sancar A: Nucleotide excision repair in human cell lines lacking both XPC and CSB proteins. Nucleic Acids Res 51: 6238-6245, 2023.
9. Zhang ET, He Y, Grob P, Fong YW, Nogales E and Tjian R: Architecture of the human XPC DNA repair and stem cell coactivator complex. Proc Natl Acad Sci U S A 112: 14817-14822, 2015.
10. Liu L, Peng Z, Xu Z and Wei X: XPC Promotes pluripotency of human dental pulp cells through regulation of Oct-4/Sox2/c-Myc. Stem Cells Int 2016: 3454876, 2016.
11. Sears CR: DNA repair as an emerging target for COPD-lung cancer overlap. Respir Investig 57: 111-121, 2019.
12. Jlassi A, Rejaibi R, Manai M, Sahraoui G, Guerfali FZ, Charfi L, Mezlini A, Manai M, Mrad K and Doghri R: VISTA/CTLA4/PD1 coexpression on tumor cells confers a favorable immune microenvironment and better prognosis in high-grade serous ovarian carcinoma. Front Oncol 14: 1352053, 2024.
13. Zhang X, He N, Gu D, Wickliffe J, Salazar J, Boldogh I and Xie J: Genetic evidence for XPC-KRAS interactions during lung cancer development. J Genet Genomics 42: 589-596, 2015.
14. Crișan AS, Tripon F, Bogliș A, Crauciuc GA, Trifa AP, Lázár E, Macarie I, Gabor MR and Bănescu C: The role of DNA repair (*XPC, XPD, XPF*, and *XPG*) gene polymorphisms in the development of myeloproliferative neoplasms. Medicina (Kaunas) 60: 506, 2024.
15. Wang W, Ma S, Ding Z, Yang Y, Wang H, Yang K, Cai X, Li H, Gao Z and Qu M: XPC protein improves lung adenocarcinoma prognosis by inhibiting lung cancer cell stemness. Front Pharmacol 12: 707940, 2021.
16. Hu LB, Chen Y, Meng XD, Yu P, He X and Li J: Nucleotide excision repair factor XPC ameliorates prognosis by increasing the susceptibility of human colorectal cancer to chemotherapy and ionizing radiation. Front Oncol 8: 290, 2018.
17. Dolatabadi S, Jonasson E, Lindén M, Fereydouni B, Bäcksten K, Nilsson M, Martner A, Forootan A, Fagman H, Landberg G, *et al*: JAK-STAT signalling controls cancer stem cell properties including chemotherapy resistance in myxoid liposarcoma. Int J Cancer 145: 435-449, 2019.
18. Chen L, Wang Y and Zhang B: Hypermethylation in the promoter region inhibits AJAP1 expression and activates the JAK/STAT pathway to promote prostate cancer cell migration and stem cell sphere formation. Pathol Res Pract 241: 154224, 2023.
19. Liu SC, Huang CM, Bamodu OA, Lin CS, Liu BL, Tzeng YM, Tsai JT, Lee WH and Chen TM: Ovatodiolide suppresses nasopharyngeal cancer by targeting stem cell-like population, inducing apoptosis, inhibiting EMT and dysregulating JAK/STAT signaling pathway. Phytomedicine 56: 269-278, 2019.
20. Loftus AEP, Romano MS, Phuong AN, McKinnel BJ, Muir MT, Furqan M, Dawson JC, Avalle L, Douglas AT, Mort RL, *et al*: An ILK/STAT3 pathway controls glioblastoma stem cell plasticity. Dev Cell 59: 3197-3212.e7, 2024.
21. Wang T, Fahrmann JF, Lee H, Li YJ, Tripathi SC, Yue C, Zhang C, Lifshitz V, Song J, Yuan Y, *et al*: JAK/STAT3-regulated fatty acid β-oxidation is critical for breast cancer stem cell self-renewal and chemoresistance. Cell Metab 27: 136-150.e5, 2018.
22. Li J, Wang Y, Wang Z, Wei Y, Diao P, Wu Y, Wang D, Jiang H, Wang Y and Cheng J: Super-enhancer driven LIF/LIFR-STAT3-SOX2 regulatory feedback loop promotes cancer stemness in head and neck squamous cell carcinoma. Adv Sci (Weinh) 11: e2404476, 2024.
23. Zhao D, Pan C, Sun J, Gilbert C, Drews-Elger K, Azzam DJ, Picon-Ruiz M, Kim M, Ullmer W, El-Ashry D, *et al*: VEGF drives cancer-initiating stem cells through VEGFR-2/Stat3 signaling to upregulate Myc and Sox2. Oncogene 34: 3107-3119, 2015.
24. Liu N, Ning X, Zhang X, Zhou Z, Fu M, Wang Y and Wu T: Gradient galectin-1 coating technology: Bionic multichannel nerve guidance conduits promote neural cell migration. Adv Technol Neurosci 1: 276-289, 2024.
25. Xiao Z, Ding L, Yu Y, Ma C, Lei C, Liu Y, Chang X, Chen Y, He Y, Zhu Y and Zhang H: Tanreqing injection inhibits stemness and enhances sensitivity of non-small cell lung cancer models to gefitinib through ROS/STAT3 signaling pathway. J Cancer 15: 4259-4274, 2024.
26. Kahnamouei SA, Narouie B, Sotoudeh M, Mollakouchekian MJ, Simforoosh N, Ziaee SA, Samzadeh M, Afshari M, Jamaldini SH, Imeni M and Hasanzad M: Association of XPC gene polymorphisms with prostate cancer risk. Clin Lab 62: 1009-1015, 2016.
27. Yang J, Xu Z, Li J, Zhang R, Zhang G, Ji H, Song B and Chen Z: XPC epigenetic silence coupled with p53 alteration has a significant impact on bladder cancer outcome. J Urol 184: 336-343, 2010.
28. Yue AM, Xie ZB, Zhao HF, Guo SP, Shen YH and Wang HP: Associations of ABCB1 and XPC genetic polymorphisms with susceptibility to colorectal cancer and therapeutic prognosis in a Chinese population. Asian Pac J Cancer Prev 14: 3085-3091, 2013.
29. MacDonagh L, Gray SG, Breen E, Cuffe S, Finn SP, O'Byrne KJ and Barr MP: Lung cancer stem cells: The root of resistance. Cancer Lett 372: 147-156, 2016.
30. Wang X, Chen Y, Wang X, Tian H, Wang Y, Jin J, Shan Z, Liu Y, Cai Z, Tong X, *et al*: Stem cell factor SOX2 confers ferroptosis resistance in lung cancer via upregulation of SLC7A11. Cancer Res 81: 5217-5229, 2021.
31. Livak KJ and Schmittgen TD: Analysis of relative gene expression data using real-time quantitative PCR and the 2(-Delta Delta C(T)) Method. Methods 25: 402-408, 2001.
32. Wang H, Huang Y, Shi J, Zhi Y, Yuan F, Yu J, Chen Z and Yang J: XPC deficiency leads to centrosome amplification by inhibiting BRCA1 expression upon cisplatin-mediated DNA damage in human bladder cancer. Cancer Lett 444: 136-146, 2019.
33. Zhao B, Huang Y, Shi J, Zhou X, Fagman JB, Wang L, Liu S, Wang W, Liu Y, Chen Z and Yang J: XPC deficiency activate cisplatin-mediated autophagy in bladder cancer by limiting novel PHRF1-mediated ubiquitination of the p53 protein. Adv Sci (Weinh) 13: e17563, 2025.
34. Wu Z, Wang M, Dong X, Sun Y, Zhang L, Tang M, Jiang X, Guo Y, Wang J, Wang W, *et al*: The deubiquitinase OTUD1 orchestrates cisplatin chemosensitivity of non-small cell lung cancer through destabilizing RAD23B/XPC. Oncogene 44: 4855-4867, 2025.
35. Lee GY, Jang JS, Lee SY, Jeon HS, Kim KM, Choi JE, Park JM, Chae MH, Lee WK, Kam S, *et al*: XPC polymorphisms and lung cancer risk. Int J Cancer 115: 807-813, 2005.
36. Zhou H, Saliba J, Sandusky GE and Sears CR: XPC protects against smoking- and carcinogen-induced lung adenocarcinoma. Carcinogenesis 40: 403-411, 2019.
37. Gao Y, Mu J, Liu K and Wang M: Integrating molecular fingerprints with machine learning for accurate neurotoxicity prediction: An observational study 2: 109-115, 2025.
38. Acharya G, Mani C, Sah N, Saamarthy K, Young R, Reedy MB, Sobol RW and Palle K: CHK1 inhibitor induced PARylation by targeting PARG causes excessive replication and metabolic stress and overcomes chemoresistance in ovarian cancer. Cell Death Discov 10: 278, 2024.
39. Manic G, Musella M, Corradi F, Sistigu A, Vitale S, Soliman Abdel Rehim S, Mattiello L, Malacaria E, Galassi C, Signore M, *et al*: Control of replication stress and mitosis in colorectal cancer stem cells through the interplay of PARP1, MRE11 and RAD51. Cell Death Differ 28: 2060-2082, 2021.
40. Liu M, Wu H and Xu C: Targeting cancer stem cell pathways for lung cancer therapy. Curr Opin Oncol 35: 78-85, 2023.
41. Wang J, Chen Y, Wang C and Ren K: Research status and controversy on non-small cell lung cancer stem cells. Adv Clin Exp Med 34: 633-640, 2025.
42. Bai Y, Xu L, Yang X, Hu Z, Yuan J, Wang F, Shao M, Yuan W, Qian J, Ma H, *et al*: Sequence variations in DNA repair gene XPC is associated with lung cancer risk in a Chinese population: A case-control study. BMC Cancer 7: 81, 2007.